Critical frontier of the Potts and percolation models on triangular-type and kagome-type lattices. II. Numerical analysis

Chengxiang Ding,[1] Zhe Fu,[1] Wenan Guo,[1,*] and F. Y. Wu[2]
[1]*Physics Department, Beijing Normal University, Beijing 100875, People's Republic of China*
[2]*Department of Physics, Northeastern University, Boston, Massachusetts 02115, USA*
(Received 7 February 2010; published 4 June 2010; publisher error corrected 14 June 2010)

In the preceding paper, one of us (F. Y. Wu) considered the Potts model and bond and site percolation on two general classes of two-dimensional lattices, the triangular-type and kagome-type lattices, and obtained closed-form expressions for the critical frontier with applications to various lattice models. For the triangular-type lattices Wu's result is exact, and for the kagome-type lattices Wu's expression is under a homogeneity assumption. The purpose of the present paper is twofold: First, an essential step in Wu's analysis is the derivation of lattice-dependent constants A,B,C for various lattice models, a process which can be tedious. We present here a derivation of these constants for subnet networks using a computer algorithm. Second, by means of a finite-size scaling analysis based on numerical transfer matrix calculations, we deduce critical properties and critical thresholds of various models and assess the accuracy of the homogeneity assumption. Specifically, we analyze the q-state Potts model and the bond percolation on the 3–12 and kagome-type subnet lattices $(n\times n):(n\times n)$, $n\leq 4$, for which the exact solution is not known. Our numerical determination of critical properties such as conformal anomaly and magnetic correlation length verifies that the universality principle holds. To calibrate the accuracy of the finite-size procedure, we apply the same numerical analysis to models for which the exact critical frontiers are known. The comparison of numerical and exact results shows that our numerical values are correct within errors of our finite-size analysis, which correspond to 7 or 8 significant digits. This in turn infers that the homogeneity assumption determines critical frontiers with an accuracy of 5 decimal places or higher. Finally, we also obtained the exact percolation thresholds for site percolation on kagome-type subnet lattices $(1\times 1):(n\times n)$ for $1\leq n\leq 6$.

DOI: 10.1103/PhysRevE.81.061111 PACS number(s): 05.50.+q, 64.60.Cn, 02.50.−r, 75.10.Hk

I. INTRODUCTION

The q-state Potts model [1,2] is a very important model in the study of phase transitions and critical phenomena. The critical frontier, or the loci of critical points, of the Potts model was first determined by Potts [1] for the square lattice. The critical exponents of the Potts model are obtained by conjectures on the basis of numerical evidence and by using Coulomb gas theory [3–7]. According to the universality hypothesis [8], the Potts model on different lattices belongs to the same universality class. But the determination of the critical frontier of the q-state Potts model in general, which includes the $q=1$ bond and site percolation, is still an outstanding challenge. Particularly, the threshold of site percolation has remained largely unresolved.

In the preceding paper [9], hereafter referred to as I, one of us (F. Y. Wu) considered the Potts model on two classes of very general two-dimensional lattices, the triangular-type and kagome-type lattices shown in Fig. 1. The Boltzmann weights W of the hatched triangles denote interactions involving 3 spins $\tau_1,\tau_2,\tau_3=1,2,\ldots,q$ surrounding a triangle, and are given by

$$W_{\triangle}(1,2,3)=A+B(\delta_{12}+\delta_{23}+\delta_{31})+C\delta_{123},$$

$$W_{\triangledown}(1,2,3)=A'+B'(\delta_{12}+\delta_{23}+\delta_{31})+C'\delta_{123}, \qquad (1)$$

where $\delta_{ij}=\delta_{\mathrm{Kr}}(\tau_i,\tau_j)$, $\delta_{123}=\delta_{12}\delta_{23}\delta_{31}$, and A, B, C, A', B', C' are constants. Spin interactions within the hatched areas can be either two- or three-site couplings. The hatched triangles can have internal structures such as the stack-of-triangle subnets, which are of recent interest [10,11], shown in Fig. 2. We refer to these structures as *subnet networks*. These stack-of-triangle lattices are called *subnet lattices*. Examples of triangular subnet lattices and kagome-type subnet lattices are shown in Figs. 2 and 3 of I. The 1×1 subnet lattices are the triangular and kagome lattices themselves. We shall call a kagome-type lattice with $m\times m$ down-pointing and $n\times n$ up-pointing subnets an $(m\times m):(n\times n)$ subnet lattice.

In paper I [9], Wu derived closed-form expressions for the critical frontier of the q-state Potts model for the 2 types of lattices in Fig. 1. For the triangular-type lattices the critical frontier is exact, but for the kagome-type lattices the critical frontier is obtained under a homogeneity assumption.

The purpose of this paper is twofold. First, an essential step in Wu's analysis is the derivation of relevant lattice-dependent constants A,B,C for subnet networks. The derivation, while elementary, is tedious. Here, we use a computer algorithm to evaluate them. Details of the algorithm are described in Sec. III.

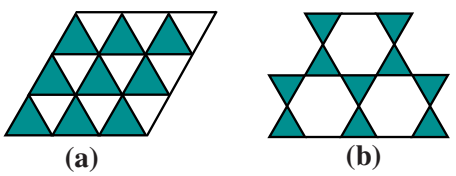

FIG. 1. (Color online) (a) Triangular-type lattice. (b) Kagome-type lattice.

*waguo@bnu.edu.cn

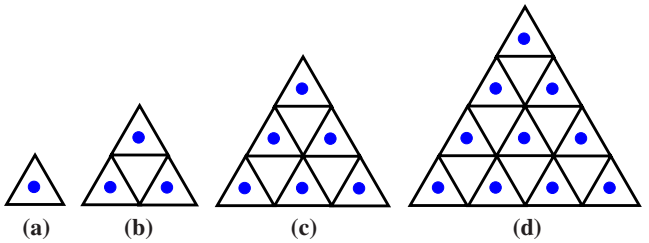

FIG. 2. (Color online) Subnet networks. (a) 1×1 subnet. (b) 2×2 subnet. (c) 3×3 subnet. (d) 4×4 subnet. The dots denote triangles with three-site interactions.

Second, we determine the critical frontier numerically and examine the accuracy of the homogeneity assumption. Specifically, we carry out a finite-size scaling analysis based on transfer matrix calculations to numerically determine the critical frontier for several lattice models, including the Potts model on the 3–12 and kagome-type $(n\times n):(n\times n)$ subnet lattices, for which the exact thresholds are not known. To assess the accuracy of the numerical determination, we also apply the procedure to models for which the exact critical thresholds are known. These include the Ising model and site percolation on the 3–12 lattice and kagome-type $(1\times1):(n\times n)$ subnet lattices, $n\leq6$. Comparison of numerical and known exact results shows that our numerical procedure is accurate to 7 or 8 decimal places. This in turn infers that the critical frontier determined using the homogeneity assumption [9] of I is accurate to 5 decimal places or higher.

Our paper is organized as follows: The main findings of paper I [9] are summarized in Sec. II. We describe in Sec. III the algorithm we use to obtain the expressions of A,B,C for the Potts model with pure two- and/or three-site subnet interactions. The resulting expressions of A,B,C are listed in the Appendix. In Sec. IV, we describe the transfer matrix technique and the finite-size scaling method. Numerical results of our transfer matrix calculations and finite-size scaling analysis are given in Sec. V. New exact thresholds are also given in Sec. V for site percolation on kagome-type $(1\times1):(n\times n)$ subnet lattices for n up to 6. We summarize our main findings in Sec. VI.

II. MAIN RESULTS OF I

We summarize in this section the main results of paper I [9]. For the triangular-type lattice shown in Fig. 1(a), the partition function is

$$Z_{\mathrm{tri}}(q;A,B,C)=\sum_{\tau_i=1}^{q}\prod_{\triangle}W_{\triangle}(i,j,k), \tag{2}$$

where the products are taken over the up-pointing triangles. Wu [9,12] showed that, in the regime

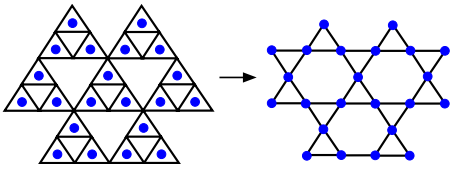

FIG. 3. (Color online) Site percolation on the kagome lattice.

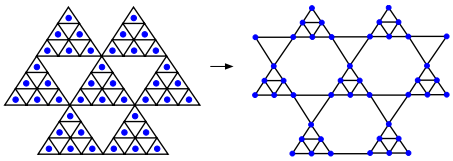

FIG. 4. (Color online) Site percolation on the $(1\times1):(2\times2)$ kagome-type subnet lattice.

$$2B+C>0,\quad 3B+C>0, \tag{3}$$

in which the ground state of $W_{\triangle}$ is ferromagnetic, the exact critical frontier is given by

$$qA=C. \tag{4}$$

The critical function Eq. (4) yields the exact thresholds of *site* percolation on lattices generated from triangular-type lattices. Consider a Potts model on a triangular subnet lattice with pure three-site interactions in dotted triangles shown in Fig. 2. Regarding faces of three-spin interactions in an $n\times n$ subnet as sites of a new lattice, the Potts model maps to a site percolation on a $(1\times1):(n-1)\times(n-1)$ kagome-type subnet lattice. The critical frontier Eq. (4) then gives the exact threshold of the site percolation. Examples of the mapping are shown in Figs. 3 and 4 for $n=2$ and 3.

For kagome-type lattices shown in Fig. 1(b) the partition function is

$$Z_{\mathrm{kag}}(q;A,B,C;A',B',C')=\sum_{\tau_i=1}^{q}\left[\prod_{\triangle}W_{\triangle}(i,j,k)\right]\times\left[\prod_{\triangledown}W_{\triangledown}(i',j',k')\right]. \tag{5}$$

Wu [9] obtained its critical frontier

$$(q^2A+3qB+C)(q^2A'+3qB'+C')-3(qB+C)(qB'+C')-(q-2)CC'=0, \tag{6}$$

under a homogeneity assumption.

The critical point in the case of $q=2$ computed from Eq. (6) is exact. Wu [9] also used Eq. (6) to compute Potts thresholds for the 3–12 and the $(m\times m):(n\times n)$ kagome-type subnet lattices for $m,n\leq4$ for which the exact thresholds are not known. In addition, Wu deduced the known exact threshold of site percolation on the 3–12 lattice by considering the Potts model on the $(2\times2):(2\times2)$ kagome-type lattice as shown in Fig. 5. In this case the homogeneity assumption turns out to give the exactly known critical frontier.

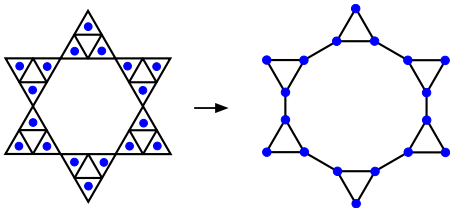

FIG. 5. (Color online) Site percolation on the 3–12 lattice.

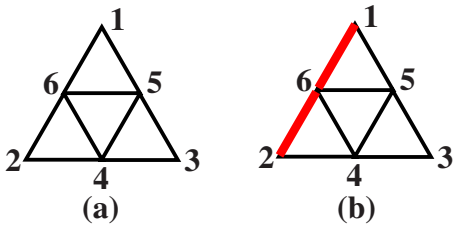

FIG. 6. (Color online) (a) 2×2 subnet with pure two-site interactions. (b) Bold (red online) bonds are occupied, other bonds are vacant.

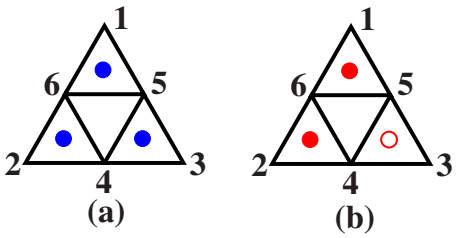

FIG. 7. (Color online) (a) 2×2 subnet with pure three-site interactions indicated by dots. (b) Solid (red online) dot denotes the dot is occupied; open dot denotes it is vacant.

III. EVALUATION OF A, B, C FOR SUBNET NETWORKS

In this section we describe the computer algorithm we use to evaluate expressions of A,B,C for the Potts model with two- and/or three-site interactions in subnet networks.

For the Potts model with two-site interactions, consider the 2×2 subnet network in Fig. 6(a) as an example. The Boltzmann weight is

$$W_{\triangle} = \sum_{\{4,5,6\}} (1+v\delta_{1,6})(1+v\delta_{1,5})(1+v\delta_{2,4})\cdots, \qquad (7)$$

where $v=e^{K}-1$, K is the two-site coupling of the Potts model.

Terms in the expansion of the products can be represented by graphs. As shown in Fig. 6(a), there are 9 bonds in the subnet. Define two states for each bond, occupied and vacant, then there are total $2^9=512$ graphs corresponding to the 512 terms in the expansion of Eq. (7). For example, Fig. 6(b) is a graph that corresponds to the term $\Sigma_{\{4,5,6\}}v\,\delta_{1,6}v\,\delta_{2,6}=q^2v^2\delta_{1,2}$ contributing to B with a term q^2v^2.

The 512 graphs are divided into five types according to following rules:

(1) Type-1, graphs with isolated spins 1, 2, and 3. The sum of these graphs generates the expression of A.

(2) Type-2, graphs with spins 1 and 2 connected and spin 3 isolated. The sum of these graphs contributes to the expression of $B\delta_{12}$. For clarity we denote it as B_{12}.

(3) Type-3, graphs with spins 2 and 3 connected and spin 1 isolated. The sum of these graphs contributes to the expression of $B\delta_{23}$ and denoted as B_{23}.

(4) Type-4, graphs with spins 3 and 1 connected and spin 2 isolated. The sum of these graphs contributes to the expression of $B\delta_{31}$ and denoted as B_{31}.

(5) Type-5, graphs with all three spins 1, 2, and 3 connected. The sum of these graphs gives rise to the expression of C.

For the Potts model with uniform and symmetric interactions, we have $B_{12}=B_{23}=B_{31}=B$.

The algorithm of our program is to generate the 512 graphs one by one, compute the weight of each graph, and classify them into the five types. The graph weight assumes the form $q^{n_c}v^{n_v}$, where n_v is the number of occupied bonds in the graph, and n_c is the number of independent clusters isolated from, i.e., not connected to, sites 1, 2, or 3. For example, the graph in Fig. 6(b) has $n_v=n_c=2$ and the weight q^2v^2.

The algorithm of our program is therefore as follows:

(1) Generate one term, i.e., a graph, by choosing a set of occupied bonds.

(2) Count the number of independent clusters isolated from site 1, 2, or 3 as n_c.

(3) Count the number of occupied bonds n_v.

(4) Assign a term $q^{n_c}v^{n_v}$ to A, B, or C according to the aforementioned rules.

(5) Go to 1 for another graph until all 512 graphs are exhausted.

The procedure for the Potts model with pure three-site interactions M is similar. Take the case shown in Fig. 7(a) as an example. The dotted up-pointing triangles have pure three-site interactions and the Boltzmann weight of the 2×2 subnet can be written as

$$W_{\triangle} = \sum_{\{4,5,6\}} (1+m\delta_{1,5,6})(1+m\delta_{2,4,6})(1+m\delta_{3,4,5}), \qquad (8)$$

where $m=e^{M}-1$.

To obtain an expansion in the form of Eq. (8), we define two states of the dots as either occupied or vacant. Thus there are $2^3=8$ graphs corresponding to the 8 terms in Eq. (8). However, up to this point, clusters are defined by the connectivity of Potts sites, *not* by the dotted faces. But the connectivity can be readily translated to that of the dotted faces. A moment's reflections shows that the weight contributing to A, B, or C is simply $q^{n_c}m^{n_m}$, where n_c is the number of independent clusters not containing sites 1, 2, or 3, and n_m is the number of occupied dots.

The rules to divide the graphs into five types corresponding to A,B,C are the same as the ones for pure two-site interactions. For example, the graph in Fig. 7(b) has $n_m=2$, $n_c=0$ and corresponds to the term $\Sigma_{4,5,6}(m\delta_{1,5,6})(m\delta_{2,4,6})=m^2\delta_{12}$, thus contributing to B_{12} with a term m^2.

The algorithm to obtain expressions of A,B,C is therefore very similar to the one described in the above for 2-site interactions. We present in the Appendix results on expressions of A,B,C for the Potts model on $n\times n$ subnets with 2-site interactions for $n\leq4$, and for subnets with three-site interactions for $n\leq7$.

IV. TRANSFER MATRIX AND FINITE-SIZE SCALING

We use the method of transfer matrix to calculate statistical variables for lattice models wrapped on a cylinder with circumference L and length N. For lattices shown in Fig. 1 with hatched triangles, L and N count up- and down-pointing

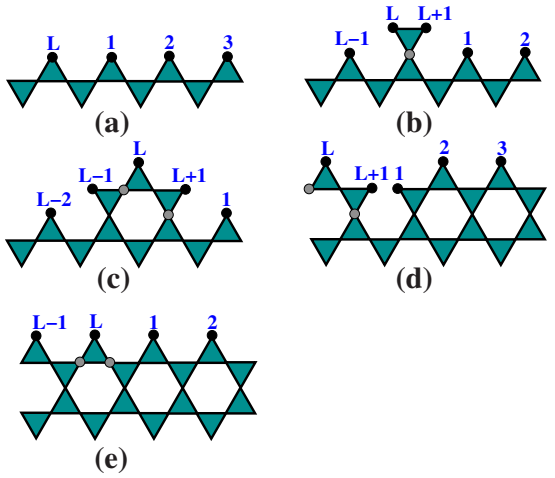

FIG. 8. (Color online) Construction of the transfer matrix for kagome-type subnet lattices. The procedure consists of several steps each corresponding to a sparse transfer matrix.

hatched triangles (rather than individual Potts spins within each triangle). Thus, for an $(m\times m):(n\times n)$ lattice shown in Fig. 8(a), there are actually $(m+n)L$ Potts spins in a length L.

For the Potts model, we build the transfer matrix by using the random-cluster representation of the Potts partition function [13,14]

$$Z=\sum_{g} v^{n_b(g)}q^{n_c(g)}, \tag{9}$$

where the summation is over all subgraphs g of the lattice (or graph) on which the Potts model is defined, $v=e^K-1$, and $n_b(g)$ and $n_c(g)$ are, respectively, the number of bonds and clusters in g. For the $(q=1)$ bond percolation we have simply $Z=(1+v)^E$, where E is the total number of edges of the lattice.

The concept of connectivity plays an essential role in the building of the transfer matrix. In the $N\times L$ cylinder, the L end sites are partitioned into clusters with sites belonging to the same cluster connected by lines. A partition is *noncrossing* if the connecting lines do not cross. Thus, there are a total of d_L noncrossing partitions. (The example of $d_4=14$ noncrossing partitions can be found in Fig. 3 of [15].) The role played by noncrossing partitions in the transfer matrix formulation of the Potts model was first noted by Temperley and Lieb [16], who found

$$d_L=\frac{1}{2L+1}\binom{2L+1}{L}. \tag{10}$$

In our transfer matrix consideration, we map and code the noncrossing partitions by a set of integers $1,2,\cdots,d_L$. A detailed explanation of the coding procedure can be found in [17].

The partition function of the Potts model can, therefore, be written as

$$Z^{(N)}=\sum_{\beta} Z_{\beta}^{(N)}, \tag{11}$$

where $Z_{\beta}^{(N)}$ is the partition sum restricted to the partition β. The restricted sums $Z_{\alpha}^{(N)}$ and $Z_{\beta}^{(N-1)}$ are connected by a transfer matrix T in the form of

$$Z_{\alpha}^{(N)}=\sum_{\beta} T_{\alpha,\beta}Z_{\beta}^{(N-1)}, \tag{12}$$

where

$$T_{\alpha,\beta}=\sum_{g} v^{\Delta n_b(g)}q^{\Delta n_c(g)} \tag{13}$$

are elements of T. Clearly, T has the dimension $d_L\times d_L$. It is also clear that the summation in Eq. (13) is over subgraphs g connecting partitions β and α of the $(N-1)$-th and Nth rows, with $\Delta n_b(g)$ and $\Delta n_c(g)$ denoting, respectively, the net (positive or negative) change of the number of bonds and clusters due to the introduction of g.

To conserve computer memory and running time, the transfer matrix is converted into a product of sparse matrices as described below (see [17] for further details). This technique has proved to be very efficient in the transfer matrix study of the Potts model, the O(n) loop and other lattice models [18–24].

The transfer matrix can be regarded as adding a new layer to the system. This process converts the transfer matrix T into a product of $L+1$ sparse matrices for kagome-type lattices of Fig. 1(b). The first sparse matrix T_1 adds one down-triangle with two "new" corner sites on top of an "old" site followed by a shift of labeling of sites. This gives rise to a new layer with $L+1$ sites as shown in Figs. 8(a) and 8(b). The matrix T_1 is a $d_{L+1}\times d_L$ rectangular matrix. The second sparse matrix T_2 adds one up- and one down-triangle simultaneously. By shifting the labels of the sites of the top (new) layer cyclically, T_2 brings in two new corner sites L and $L+1$ on top of the current layer, and covers two old corner sites $L+1$ and 1, as shown in Figs. 8(b) and 8(c). T_2 is a $d_{L+1}\times d_{L+1}$ square matrix. After $L-1$ such steps, the graph is transformed to the one shown in Fig. 8(d). By adding an up-triangle on the two old sites $L+1$ and 1 under cylindrical boundary condition, the last sparse matrix T_3 adds the last new corner site L to the system as shown from Figs. 8(d) and 8(e). Labels of the top sites are shifted and T_3 is a $d_L\times d_{L+1}$ rectangular matrix.

The transfer matrix T now assumes the form of a product of sparse matrices,

$$T=T_3T_2^{L-1}T_1. \tag{14}$$

In the actual calculation, we need to store only the positions and values of the nonzero elements of each sparse matrix in a few one-dimensional arrays.

In constructing these sparse matrices, one needs to enumerate all possible graphs inside the added (one or two) hatched triangles for a given connectedness of the partitions of the new and old layers. For example, in the construction of T_1, we need to add a subnet shown in Fig. 2 (flipped vertically). In the case of 1×1 subnet, it is straightforward to enumerate all graphs manually. However, in the case of 2

$\times 2$ and higher order subnets, it is tedious and sometimes impossible to count all possible graphs by hand. Therefore, we make use of a computer algorithm similar to the one used in obtaining expressions of A,B,C to count Δn_b and Δn_c.

For site percolation, the partition function is

$$Z = \sum_g s^{n_s(g)}(1-s)^{N-n_s(g)} = 1, \tag{15}$$

where the summation is over all site percolation configurations g, s is the probability that a site is occupied, $n_s(g)$ is the number of occupied sites in g, and N is the total number of sites. The corresponding transfer matrix is defined in a way similar to that of the Potts model, but with a twist due to the presence of vacant sites and henceforth not all L end sites are occupied. Denote the number of end sites that are occupied by $n=0,1,\cdots,L$ which can be distributed in $\binom{L}{n}$ different ways. Then there are a total of

$$d_L^S = \sum_{n=0}^{L} \binom{L}{n} d_n \tag{16}$$

non-crossing partitions and the transfer matrix has the dimension $d_L^S \times d_L^S$. It is clear that we have $d_L^S > d_L$.

The partitions can again be coded by means of a sequence of integers $1,2,\cdots,d_L^S$. The coding algorithm is the same as that used in the consideration of the Potts model with vacancies [19] and in the study of site percolation [25].

To determine the critical threshold of the Potts model and/or site percolation, we calculate the magnetic scaled gap

$$X_h(v,L) = \frac{L}{2\pi\xi_h(v,L)}, \tag{17}$$

where $\xi_h(v,L)$ is the magnetic correlation length (with v replaced by s for site percolation). In the language of the random cluster model and site percolation, the magnetic correlation function is defined to be the probability that two sites at a distance r belong to the same cluster, or

$$g_r = \frac{Z'}{Z}, \tag{18}$$

where $Z' = \Sigma_g v^{n_b(g)} q^{n_c(g)}$ for the random cluster model and $Z' = \Sigma_g s^{n_s(g)}(1-s)^{N-n_s(g)}$ for site percolation. The summations in Z' are the same as in Eqs. (9) and (15) but restricted to subgraphs g with at least one cluster spanning from row 1 to row r.

We define a transfer matrix, hereafter referred to as the magnetic sector of the transfer matrix, based on Z', in a way similar to that of the transfer matrix based on Z in Eq. (13) and (15) in the "nonmagnetic" sector. In constructing the magnetic sector of the transfer matrix, we use the "magnetic" type connectivity of the L end sites of the cylinder, which, in addition to describing how sites are connected, specifies which sites are still connected to a site in row 1. These sites are called "magnetic sites." To count the total number of noncrossing partitions describing the magnetic type connectivity, we first code the positions of the magnetic sites by means of a binary number $m=0,1,\ldots,2^L-1$, where the binary digit 1 denotes a magnetic site. The magnetic sites divide the remaining sites in $g(m)$ groups such that two sites in different groups cannot be connected. Let $n(j)$ be the number of sites in the jth group. Then there are

$$h_m = d_{n(1)} d_{n(2)} \cdots d_{n(g(m))} \tag{19}$$

noncrossing partitions for the Potts model and

$$h_m^S = d_{n(1)}^S d_{n(2)}^S \cdots d_{n(g(m))}^S \tag{20}$$

noncrossing partitions for site percolation. The total number of noncrossing partitions is therefore

$$d_L^{(m)} = \sum_{m=0}^{2^L-1} h_m \tag{21}$$

for the Potts model, and

$$d_L^{S(m)} = \sum_{m=0}^{2^L-1} h_m^S \tag{22}$$

for the site percolation.

The partitions can again be coded by means of a sequence of integers. A detailed description of the coding algorithm can be found in [19]. The magnetic sectors of the transfer matrix now have the dimensions $d_L^{(m)} \times d_L^{(m)}$ and $d_L^{S(m)} \times d_L^{S(m)}$ for the Potts model and site percolation, respectively, and are much larger than those of the nonmagnetic sectors. The magnetic sector of the transfer matrix can also be converted into a product of sparse matrices in the same way as in the case of the nonmagnetic sector.

The inverse magnetic correlation length is given by

$$\frac{1}{\xi_h(v,L)} = \zeta \ln\left(\frac{\lambda_0}{\lambda_0'}\right), \tag{23}$$

where λ_0 and λ_0' are the leading eigenvalues of the transfer matrix in the nonmagnetic and magnetic sector, respectively, ζ is a geometrical factor which is the ratio between the unit of L and the thickness of a layer added by the transfer matrix. The magnetic scaled gap then follows.

According to finite-size scaling theory [26] and Cardy's conformal mapping [27], $X_h(v,L)$ can be expanded as

$$X_h(v,L) = X_h + atL^{y_t} + buL^{y_u} + \ldots, \tag{24}$$

where X_h is the magnetic scaling dimension, t is the deviation from the critical point, and u the irrelevant field. Here, y_t is the thermal renormalization exponent, y_u the leading irrelevant renormalization exponent, and a and b are unknown constants.

We substitute Eq. (24) into the finite-size scaling equation connecting lattices of sizes L and $L-1$,

$$X_h(v,L) = X_h(v,L-1), \tag{25}$$

and denote the solution of Eq. (25) by $v_c(L)$, which has the expansion

$$v_c(L) = v_c + a'uL^{y_u - y_t} + \cdots, \tag{26}$$

where a' is an unknown constant. Because $y_u < 0$ and $y_t > 0$, $v_c(L)$ for a sequence of increasing system sizes converge to the critical point v_c.

TABLE I. Critical properties of the Potts model on the 3–12 lattice. (H=Homogeneity Assumption, N=Numerical, and T=Theoretical universality prediction.)

q	v_c (H)	v_c (N)	c (T)	c (N)	X_h (T)	X_h (N)
0.5	2.007916417382387	2.00788(1)	−0.445833945	−0.4458340(1)	0.082757037	0.08276(1)
1.0	2.852426157798754	2.8523883(2)	0	0	0.104166667	0.104167(1)
1.5	3.510849695265078	3.510825(2)	0.288024142	0.288024(1)	0.116778423	0.116778(1)
2.0	4.073446135573680	4.0734460(1)	0.5	0.500000(1)	1/8	0.12500000(1)
2.5	4.574927577671523	4.574952(3)	0.66584083	0.66585(1)	0.130338138	0.13033(1)
3.0	5.033022514872745	5.033077(3)	4/5	0.800(1)	2/15	0.13333(1)
3.5	5.458234413883058	5.458313(2)	0.910294591	0.91(1)	0.133771753	0.1339(3)
4.0	5.857394827983647	5.857497(3)	1	0.999(1)	1/8	0.13(1)

At $v_c(L)$, the expression $X_h[v_c(L),L]$ for a sequence of sizes L converges to the magnetic scaling dimension X_h as

$$X_h(v_c(L),L) = X_h + b' u L^{y_u} + \ldots, \tag{27}$$

with b' an unknown constant. This determines the magnetic scaling dimension X_h.

The free energy per unit area is given by

$$f(L) = \frac{\zeta \ln \lambda_0}{L}, \tag{28}$$

where λ_0 is the largest eigenvalue of the transfer matrix in the nonmagnetic sector. According to conformal invariance theory, the large-L asymptotic finite-size behavior of the free energy density at the critical point is [28,29]

$$f(L) \simeq f(\infty) + \frac{\pi c}{6L^2}, \tag{29}$$

where c is the conformal anomaly.

The conformal anomaly c and the magnetic scaling dimension X_h are two important universal quantities defining the universality class. For the two-dimensional q-state Potts model, they are given by the conformal invariance theory and Coulomb gas method [3,4,28–30] as

$$c = 1 - \frac{6(1-g)^2}{g}, \quad X_h = 1 - \frac{g}{2} - \frac{3}{8g}, \tag{30}$$

where

$$\sqrt{q} = -2\cos(\pi g), \quad \tfrac{1}{2} \le g \le 1. \tag{31}$$

V. NUMERICAL AND SOME EXACT RESULTS

In this section, we present numerical results of our transfer matrix calculations and finite-size scaling analysis for the 3–12 and kagome-type lattices. We also present some exact results for site percolation on the $(1\times1):(n\times n)$ lattices.

A. q-state Potts model on the 3–12 and kagome-type subnet lattices

Critical points are estimated by extrapolating the solutions of Eq. (25) for a sequence of increasing system sizes in accordance with the finite-size scaling Eq. (26). The numerical accuracy one reaches depends highly on the system size reached in the calculation.

For the 3–12 lattice and the $(1\times1):(1\times1)$ (the kagome) and $(2\times2):(2\times2)$ kagome-type subnet lattices, the largest dimension of the arrays used to store the values and the positions of nonzero elements of the sparse matrices is $d_{L+1}^{(m)}$. The largest system size we reached is $L=15$ with $d_{16}^{(m)}=335897865$. For the $(3\times3):(3\times3)$ and $(4\times4):(4\times4)$ kagome-type subnet lattices, the sparse matrix T_2 in the magnetic sector is further decomposed in two rectangular matrices of dimensions $d_{L+1}^{(m)}\times d_{L+2}^{(m)}$ and $d_{L+2}^{(m)}\times d_{L+1}^{(m)}$, and the largest system size we reached is $L=14$. The computer memory requirement for the calculations of the largest system is about

TABLE II. Critical properties of the Potts model on the kagome (1×1) lattice. (H=Homogeneity Assumption, N=Numerical, and T=Theoretical universality prediction.)

q	v_c (H)	v_c (N)	c (T)	c (N)	X_h (T)	X_h (N)
0.5	0.787417375457453	0.787320(1)	−0.445833945	−0.445834(1)	0.082757037	0.082757(1)
1.0	1.102738621067509	1.10262924(2)	0	0	0.104166667	0.104167(1)
1.5	1.342082948593078	1.3420126(2)	0.288024142	0.2880243(3)	0.116778423	0.116780(3)
2.0	1.542459756837412	1.5424598(1)	0.5	0.500000(1)	1/8	0.12500000(1)
2.5	1.718102046569530	1.718191(3)	0.66584083	0.66584(1)	0.130338138	0.1304(1)
3.0	1.876269208345760	1.876458(3)	4/5	0.8000(1)	2/15	0.1333(1)
3.5	2.021253955272383	2.02154(2)	0.910294591	0.910(1)	0.133771753	0.134(1)
4.0	2.155842236513638	2.15620(5)	1	1.00(1)	1/8	0.13(1)

TABLE III. Critical properties of the Potts model on the $(2\times2):(2\times2)$ kagome lattice. (H=Homogeneity Assumption, N=Numerical, and T=Theoretical universality prediction.)

q	v_c (H)	v_c (N)	c (T)	c (N)	X_h (T)	X_h (N)
0.5	1.115482279992555	1.1154309(3)	−0.445833945	−0.4458340(2)	0.082757037	0.082757(1)
1.0	1.505450910604828	1.5053987(1)	0	0	0.104166667	0.104167(1)
1.5	1.790803965420646	1.7907720(2)	0.288024142	0.288024(1)	0.116778423	0.11678(1)
2.0	2.024382957091806	2.02438295(3)	0.5	0.500000(1)	1/8	0.1250000(1)
2.5	2.225885325024986	2.2259229(2)	0.66584083	0.66584(1)	0.130338138	0.13034(1)
3.0	2.405138877193783	2.4052181(3)	4/5	0.8001(1)	2/15	0.1333(1)
3.5	2.567855953492942	2.567981(2)	0.910294591	0.910(1)	0.133771753	0.1339(3)
4.0	2.717691692682905	2.717856(2)	1	0.99(1)	1/8	0.13(1)

65 gigabytes, which is quite large, but the CPU time consumed is rather modest. It is just a few hours for a typical calculation of the magnetic scaled gap.

The magnetic scaling dimension X_h is estimated by extrapolating the scaled gaps $X_h(v_c(L),L)$ at the solution of Eq. (25) for a sequence of increasing system sizes in accordance with Eq. (27). The free energy density at the estimated critical point is calculated using Eq. (28) and the conformal anomaly c is computed by making use of the finite-size scaling relation Eq. (29). Details of the data fitting procedure are described in [17]. We also checked corrections to scaling due to the leading irrelevant field. Take the simple kagome lattice as an example. According to the Coulomb gas theory [30], $y_{t_2}=4-4/g$ with g given in Eq. (31) is the second leading thermal exponent, which we expect to be a candidate for the leading correction exponent y_u. For $q>2$, we indeed found y_u close to y_{t_2}. For $q=0.5$, y_u is about −2.00(1), which is the analytic one. For $q=1.0$ and 1.5, we found $y_u=-1.79(3)$ and −1.51(2), respectively, which dominate and overcome the corresponding y_{t_2}. For $q=2$, the Ising model, we obtain $y_u=-4.00(1)$. The amplitudes of $y_{t_2}=-4/3$ and the analytic $y_u=-2$ corrections vanish. This is understandable for lattices with sixfold rotational symmetry. This picture is generally true for all $(n\times n):(n\times n)$ kagome subnet lattices.

We summarize in Tables I–V numerical results of our calculations on the critical point v_c, conformal anomaly c, and magnetic scaling dimension X_h together with the universality predictions of c and X_h. We have also computed v_c using the homogeneity assumption and list the results. The v_c calculation for the kagome lattice extends those of [31] using Monte Carlo renormalization group method and finite-site scaling analysis for $q=1,2,3,4$. Our study extends to noninteger q and offers results with higher accuracy.

For $q=2$, the Ising model, our numerical estimates of the critical threshold agree with the exact critical results up to 7 or 8 decimal numbers. This probably indicates the limit of the numerical accuracy of the finite-size analysis we can reach at present. For $q\neq2$, the critical points obtained from Eq. (6) under the homogeneity assumption coincide with our numerical estimations to 5 or so decimal places but lie outside error bars. This indicates that the homogeneity assumption, while highly accurate, is an excellent approximation yielding numerical values with an error within one part in 10^5. Our computed values of the conformal anomaly c and the magnetic scaling dimension X_h coincide with the theoretical universality predictions within error bars.

Our numerical results for bond percolation are summarized in Table VI for the 3–12 lattice and the $(n\times n):(n\times n)$ subnet kagome-type lattices. For the kagome lattice, we found $p_c=0.524404978(5)$, which coincides with the best estimation [25]. For the 3–12 lattice our numerical result of $p_c=0.74042077(2)$ is in agreement with other findings [11,33,34] to 6 decimal places. For kagome-type subnet lattices, our numerical analysis determines p_c with an accuracy up to 7 or 8 decimal places.

TABLE IV. Critical properties of the Potts model on the $(3\times3):(3\times3)$ kagome lattice. (H=Homogeneity Assumption, N=Numerical, and T=Theoretical universality prediction.)

q	v_c (H)	v_c (N)	c (T)	c (N)	X_h (T)	X_h (N)
0.5	1.236699591471530	1.2366855(3)	−0.445833945	−0.4458340(2)	0.082757037	0.0827569(2)
1.0	1.626971272019731	1.6269594(2)	0	0	0.104166667	0.104167(1)
1.5	1.906766682469675	1.906760(1)	0.288024142	0.288024(1)	0.116778423	0.116779(2)
2.0	2.133002727374153	2.13300273(1)	0.5	0.500000(1)	1/8	0.1250000(1)
2.5	2.326449318777172	2.32645568(5)	0.66584083	0.66585(1)	0.130338138	0.130338(1)
3.0	2.497336478778200	2.4973486(2)	4/5	0.800(1)	2/15	0.1333(1)
3.5	2.651556985414795	2.651575(3)	0.910294591	0.91(1)	0.133771753	0.1338(1)
4.0	2.79285603450327	2.79288(2)	1	0.999(1)	1/8	0.13(1)

TABLE V. Critical properties of the Potts model on the $(4\times4):(4\times4)$ kagome lattice. (H=Homogeneity Assumption, N=Numerical, and T=Theoretical universality prediction.)

q	v_c (H)	v_c (N)	c (T)	c (N)	X_h (T)	X_h (N)
0.5	1.287715536704650	1.2877116(2)	−0.445833945	−0.4458340(1)	0.082757037	0.0827569(1)
1.0	1.669262339202358	1.6692593(3)	0	0	0.104166667	0.10417(1)
1.5	1.941284616762751	1.9412832(5)	0.288024142	0.288024(1)	0.116778423	0.11678(1)
2.0	2.160721132019555	2.160721132(1)	0.5	0.500000(1)	1/8	0.1250000(1)
2.5	2.348099505779181	2.3481001(2)	0.66584083	0.66585(1)	0.130338138	0.13034(1)
3.0	2.513467694176093	2.5134684(2)	4/5	0.800(1)	2/15	0.1333(1)
3.5	2.662592230189568	2.662594(3)	0.910294591	0.911(1)	0.133771753	0.134(1)
4.0	2.799129506399588	2.799132(5)	1	0.999(1)	1/8	0.13(1)

In Table VI, we also give thresholds computed using the homogeneity assumption Eq. (6). The polynomial equations determining the bond percolation thresholds p_c under the homogeneity assumption Eq. (6) for $(n\times n):(n\times n)$ subnet lattices in Table VI are as follows:

$$1-3p^2-6p^3+12p^4-6p^5+p^6=0,\quad (n=1), \tag{32}$$

$$1-3p^4-18p^5-39p^6+30p^7+273p^8+264p^9-1785p^{10}-126p^{11}+8232p^{12}-162326p^{13}+16359p^{14}-9948p^{15}+3708p^{16}-786p^{17}+73p^{18}=0,\quad (n=2), \tag{33}$$

$$1-3p^6-36p^7-186p^8-372p^9+447p^{10}+3558p^{11}+4711p^{12}-5274p^{13}-30771p^{14}-110816p^{15}+69828p^{16}+1309302p^{17}-242760p^{18}-10117626p^{19}+9190737p^{20}+53446600p^{21}-137597577p^{22}-15101358p^{23}+714425889p^{24}-1897059306p^{25}+2985201585p^{26}-3337272356p^{27}+2817156177p^{28}-1840940730p^{29}+938230487p^{30}-371179194p^{31}+112125462p^{32}-25052124p^{33}+3909120p^{34}-380880p^{35}+17464p^{36}=0,\quad (n=3), \tag{34}$$

$$1-3p^8-60p^9-528p^{10}-2406p^{11}-4518p^{12}+8388p^{13}+64323p^{14}+108744p^{15}-149520p^{16}-892404p^{17}-664532p^{18}+2272086p^{19}-2348817p^{20}-12425874p^{21}+123063933p^{22}+344663478p^{23}-1382031989p^{24}-5244471786p^{25}+12598666671p^{26}+50539880448p^{27}-112896871341p^{28}-350902330710p^{29}+955575283123p^{30}+1782743557128p^{31}-7239409905561p^{32}-5767231526534p^{33}+52365034246041p^{34}-23401813013430p^{35}-353073527306441p^{36}+1041090144149322p^{37}-623756767891383p^{38}-4367477247915326p^{39}+18117607172859264p^{40}-42034422047996604p^{41}+71675099615055545p^{42}-97479081216503664p^{43}+109775262989475858p^{44}-104474772230850020p^{45}+85036825023972936p^{46}-59604466077733650p^{47}+36101308809040333p^{48}-18909591474961260p^{49}+8552494666923729p^{50}-3327421649714158p^{51}+1106659102637175p^{52}-311767535257674p^{53}+73442507365712p^{54}-14206464131418p^{55}+2198697552561p^{56}-261883431344p^{57}+22544948382p^{58}-1248899580p^{59}+33437353p^{60}=0,\quad (n=4). \tag{35}$$

The threshold Eq. (32) for $n=1$ has previously been given in [31,35] and in [33,36]. Thresholds Eqs. (33)–(35) for $n=2,3,4$ are new. The polynomial equation determining p_c under the homogeneity assumption in Table VI for the 3–12 lattice has been given in paper I [9,36], and is $1-p+p^2+p^3-7p^4+4p^5=0$.

B. Site percolation on the 3–12 lattice

The exact critical threshold for site percolation on the 3–12 lattice is known to be $s_c=\sqrt{1-2\sin(\pi/18)}$. It was first given in [37] and is shown in paper I [9] to be the same as that of the $(2\times2):(2\times2)$ Potts subnet lattice with pure three-site interactions. To calibrate our numerical approach, we have also computed s_c using the transfer matrix approach. Our numerical determination of critical properties of site percolation is summarized in the last row in Table VII. The comparison of numerical estimates of thresholds with exact results shows agreements up to 7 decimal places (within errors), indicating our numerical estimates to be accurate to the same degree of accuracy. Our numerical determination of the

TABLE VI. The thresholds p_c of bond percolation on the 3–12 and various kagome-type subnet lattices. (H=Homogeneity Assumption and N=Numerical.)

Subnet	p_c (H)	p_c (N)	Other sources
$(1\times1):(1\times1)$	0.524429717521274	0.524404978(5)	0.52440499(2)[a]
(kagome lattice)			0.52440503(5)[a]
			0.5244053(3)[b]
$(2\times2):(2\times2)$	0.600870248238631	0.60086193(3)	0.6008624(10)[c]
$(3\times3):(3\times3)$	0.619333484666866	0.61933176(5)	0.6193296(10)[c]
$(4\times4):(4\times4)$	0.625364661497144	0.62536424(7)	0.625365(3)[c]
3–12 lattice	0.740423317919897	0.74042077(2)	0.74042118[d]
			0.74042081[c]
			0.74042195(80)[e]

[a]Reference [25].
[b]Reference [32].
[c]Reference [11].
[d]Reference [33].
[e]Reference [34].

conformal anomaly and magnetic scaling dimension of site percolation indicates that these models all belong to the two-dimensional $q=1$ Potts model universality class. Again, the hypothesis of universality is verified.

C. Exact thresholds for site percolation on the $(1\times1):(n\times n)$ kagome-type lattice

It was shown in paper I [9], and in Sec. II, that the rigorous critical frontier Eq. (4) yields the exact thresholds of site percolation on $(1\times1):(n\times n)$ kagome-type subnet lattices. The polynomial equations determining the threshold s_c are generated by substituting expressions of A and C in Eqs. (A.5)–(A.11) into Eq. (4) and setting $q=1$. This yields the site percolation thresholds shown in Table VII. Explicitly, the thresholds for site percolation on $(1\times1):(n\times n)$ kagome-type subnet lattices, $1\leq n\leq 6$, in Table VII are as follows:

$$1-3s^2+s^3=0, \quad (n=1) \tag{36}$$

$$1-3s^3-3s^4+6s^5-2s^6=0, \quad (n=2) \tag{37}$$

$$1-3s^4-9s^5+9s^6+11s^7-12s^8+s^9+s^{10}=0, \quad (n=3) \tag{38}$$

$$1-3s^5-18s^6+12s^7+12s^8+41s^9-66s^{10}+9s^{11}-9s^{12}+48s^{13}-36s^{14}+8s^{15}=0, \quad (n=4) \tag{39}$$

$$1-3s^6-30s^7+60s^9-30s^{10}+216s^{11}-329s^{12}-48s^{13}+3s^{14}+396s^{15}+180s^{16}-1113s^{17}+1038s^{18}-393s^{19}+48s^{20}+3s^{21}=0, \quad (n=5) \tag{40}$$

$$1-3s^7-45s^8-45s^9+165s^{10}-75s^{11}+165s^{12}+510s^{13}-1056s^{14}-959s^{15}+367s^{16}+2349s^{17}+3433s^{18}-6589s^{19}-9069s^{20}+22070s^{21}-11495s^{22}-3597s^{23}+4455s^{24}+702s^{25}-1971s^{26}+792s^{27}-106s^{28}=0, \quad (n=6). \tag{41}$$

TABLE VII. Critical properties of site percolation on $(1\times1):(n\times n)$ kagome-type subnet lattices and the 3–12 lattice. (E=Exact result, N=Numerical, and T=Theoretical universality prediction.)

Subnet	s_c (E)	s_c (N)	Other sources	$c(T)$	$c(N)$	X_h (T)	X_h (N)
$(1\times1):(1\times1)$	0.652703644666139	0.6527035(2)	$1-2\sin(\pi/18)$[a]	0	0	0.1041667	0.1042(1)
$(1\times1):(2\times2)$	0.707106781186548	0.7071068(2)	$1/\sqrt{2}$[b]	0	0	0.1041667	0.10416(1)
$(1\times1):(3\times3)$	0.728355596425196	0.7283555(1)		0	0	0.1041667	0.10417(1)
$(1\times1):(4\times4)$	0.738348473943256	0.7383483(5)		0	0	0.1041667	0.10417(2)
$(1\times1):(5\times5)$	0.743548682503071	0.7435486(3)		0	0	0.1041667	0.1042(1)
$(1\times1):(6\times6)$	0.746418147634282	0.7464180(3)		0	0	0.1041667	0.10417(1)
3–12 lattice	$\sqrt{1-2\sin(\pi/18)}=0.807900764120$	0.8079008(3)	$\sqrt{1-2\sin(\pi/18)}$[c]	0	0	0.1041667	0.10416(1)
			0.807904(4) [N][c]				

[a]Reference [38].
[b]Reference [39].
[c]Reference [37].

The threshold $s_c=1-2\sin(\pi/18)$ for the $n=1$ kagome lattice was first given in [38]. The threshold $s_c=1/\sqrt{2}$ for $n=2$ has also been obtained by a "cell-to-cell" transformation in [39]. Here, the thresholds for $3\leq n\leq 6$ are new.

We also computed s_c and other critical properties numerically. The results are summarized in Table VII. Again, our numerical estimates of s_c agree with the exact results up to 7 decimal places, and these models all belong to the two-dimensional $q=1$ Potts model universality class.

Finally, we comment on some numerical specifics. Since the number of noncrossing partitions for site percolation is much larger than that of the Potts model in both the magnetic and nonmagnetic sector for a given circumference L, the maximum system size $L=12$ that we reached is smaller. The largest dimension of arrays used to save values and positions of nonzero elements of the sparse matrices is $d_{L=13}^{S(m)}=125481607$, which requires about 43 gigabytes computer memory in the calculations. Corrections to scaling due to the leading irrelevant field is about $-1.8(1)$ for all lattices.

VI. SUMMARY

We have studied critical properties of the q-state Potts model and bond and site percolation on two general classes of lattices, the triangular-type and kagome-type lattices. For the triangular-type lattices of Fig. 1(a), the exact critical frontier is known and this led to a determination of the exact critical thresholds of site percolation on $(1\times 1):(n\times n)$ kagome-type subnet lattices. Results for $1\leq n\leq 6$ are given. For the kagome-type lattices of Fig. 1(b), no exact results are known except for $q=2$. We carried out finite-size analysis to numerically determine critical properties for various lattice models including the 3–12 lattice and $(n\times n):(n\times n)$ kagome-type subnet lattices. Our numerical results on conformal anomaly and magnetic correlation length verify that the principle of universality holds.

We have also computed the critical thresholds for the Potts and bond percolation on the 3–12 lattice and $(n\times n):(n\times n)$ kagome-type subnet lattices using the homogeneity assumption Eq. (6). To assess the accuracy of our numerical analysis as well as that of the homogeneity assumption, we have applied our numerical procedure to study critical properties of models for which exact results are known. The comparison of numerical and known results shows that the numerical procedure is accurate within errors of our finite-size analysis, which correspond to 7 or 8 significant digits, in determining critical thresholds. Assuming the same degree of accuracy for all lattice, this in turn infers that the homogeneity assumption determines critical threshold with an accuracy up to 5 decimal places or higher. The only way the precision could be worse is if the finite-size scaling procedure suffered from additional systematic effects not estimated by the errors.

Finally, our analysis of critical properties is based on the use of lattice-dependent constants A,B,C for the hatched triangles shown in Fig. 1. We have developed an algorithm of evaluating expressions of A,B,C using computers for hatched triangles in the form of a stack-of-triangle structure.

ACKNOWLEDGMENTS

F.Y.W. would like to thank Professor Z. G. Zheng for the hospitality at the Beijing Normal University. W.G. is much indebted to H. W. J. Blöte for valuable discussions. We thank R. M. Ziff for valuable comments and sending a copy of Ref. [36] prior to publication. This work is supported by the National Science Foundation of China (NSFC) under Grant No. 10675021, by the Program for New Century Excellent Talents in University (NCET), and by the High Performance Scientific Computing Center (HSCC) of the Beijing Normal University.

APPENDIX: EXPRESSIONS OF A,B,C

In this appendix we list constants A,B,C computed using the computer algorithm as described in Sec. III. The condition Eq. (3) holds for ferromagnetic Potts models with $v,m,q>0$. This confirms that $qA=C$ is the exact critical frontier in the ferromagnetic regime.

1. Potts model on $n\times n$ subnets with pure 2-site coupling K

$$v=e^K-1$$

Subnet 1×1:

$$A=1,\quad B=v,\quad C=v^3+3v^2. \tag{A.1}$$

Subnet 2×2:

$$A=q^3+9q^2v+33qv^2+(50+4q)v^3+21v^4+3v^5$$

$$B=q^2v^2+10qv^3+(30+2q)v^4+22v^5+7v^6+v^7$$

$$C=9qv^4+(54+3q)v^5+63v^6+33v^7+9v^8+v^9. \tag{A.2}$$

Subnet 3×3:

$$A=29q^3v^6+(459q^2+9q^3)v^7+(2592q+423q^2)v^8+(5292+4185q+171q^2)v^9+(12825+3258q+36q^2)v^{10}+(15534+1539q+3q^2)v^{11}+(12184+454q)v^{12}+(6732+78q)v^{13}+(2688+6q)v^{14}+768v^{15}+150v^{16}+18v^{17}+v^{18},$$

$$B=q^5v^3+21q^4v^4+(199q^3+3q^4)v^5+(1040q^2+85q^3)v^6+(2979q+844q^2+17q^3)v^7+(3780+3834q+340q^2+2q^3)v^8+(7182+2429q+86q^2)v^9+(6858+950q+13q^2)v^{10}+(4250+233q+q^2)v^{11}+(1846+33q)v^{12}+(570+2q)v^{13}+121v^{14}+16v^{15}+v^{16},$$

$$C = 29q^3v^6 + (459q^2 + 9q^3)v^7 + (2592q + 423q^2)v^8 + (5292 + 4185q + 171q^2)v^9 + (12825 + 3258q + 36q^2)v^{10} + (15534 + 1539q + 3q^2)v^{11} + (12184 + 454q)v^{12} + (6732 + 78q)v^{13} + (2688 + 6q)v^{14} + 768v^{15} + 150v^{16} + 18v^{17} + v^{18}. \quad \text{(A.3)}$$

Subnet 4×4:

$$A = q^{12} + 30q^{11}v + 435q^{10}v^2 + (4044q^9 + 16q^{10})v^3 + (26952q^8 + 450q^9)v^4 + (136323q^7 + 6057q^8 + 18q^9)v^5 + (539687q^6 + 51643q^7 + 606q^8)v^6 + (1696074q^5 + 310764q^6 + 9336q^7 + 27q^8)v^7 + (4229307q^4 + 1388580q^5 + 88062q^6 + 948q^7)v^8 + (8218405q^3 + 4700302q^4 + 568443q^5 + 15274q^6 + 43q^7)v^9 + (11888619q^2 + 11989938q^3 + 2635653q^4 + 148602q^5 + 1608q^6)v^{10} + (11554638q + 22208904q^2 + 8874255q^3 + 966189q^4 + 26310q^5 + 96q^6)v^{11} + (5728860 + 27132098q + 21124723q^2 + 4354609q^3 + 251967q^4 + 3222q^5 + 3q^6)v^{12} + (16691130 + 32535501q + 13440978q^2 + 1559913q^3 + 48486q^4 + 267q^5)v^{13} + (24925347 + 26263347q + 6337347q^2 + 426225q^3 + 6834q^4 + 12q^5)v^{14} + (25218686 + 15860794q + 2323668q^2 + 89613q^3 + 644q^4)v^{15} + (19264962 + 7537923q + 674634q^2 + 14088q^3 + 30q^4)v^{16} + (11718378 + 2882733q + 154248q^2 + 1539q^3)v^{17} + (5825765 + 890008q + 27036q^2 + 102q^3)v^{18} + (2389554 + 219258q + 3447q^2 + 3q^3)v^{19} + (806778 + 42009q + 288q^2)v^{20} + (221570 + 5996q + 12q^2)v^{21} + (48435 + 594q)v^{22} + (8136 + 36q)v^{23} + (990 + q)v^{24} + 78v^{25} + 3v^{26},$$

$$B = q^9v^4 + 36q^8v^5 + (609q^7 + 4q^8)v^6 + (6340q^6 + 193q^7)v^7 + (44883q^5 + 3730q^6 + 30q^7)v^8 + (225145q^4 + 40957q^5 + 1156q^6 + 3q^7)v^9 + (804174q^3 + 290085q^4 + 19521q^5 + 240q^6)v^{10} + (1980543q^2 + 1384197q^3 + 192846q^4 + 6208q^5 + 30q^6)v^{11} + (3064302q + 4394962q^2 + 1220478q^3 + 85315q^4 + 1355q^5 + 2q^6)v^{12} + (2280420 + 8560443q + 4979114q^2 + 717391q^3 + 26906q^4 + 201q^5)v^{13} + (7901226 + 12201635q + 3771317q^2 + 307105q^3 + 6145q^4 + 19q^5)v^{14} + (14006718 + 11666444q + 2106366q^2 + 99167q^3 + 989q^4 + q^5)v^{15} + (16765996 + 8289847q + 906964q^2 + 24293q^3 + 102q^4)v^{16} + (15077600 + 4592110q + 306788q^2 + 4431q^3 + 5q^4)v^{17} + (10735261 + 2026213q + 81784q^2 + 574q^3)v^{18} + (6217796 + 715829q + 17041q^2 + 48q^3)v^{19} + (2966339 + 200961q + 2720q^2 + 2q^3)v^{20} + (1168690 + 43935q + 319q^2)v^{21} + (378274 + 7210q + 25q^2)v^{22} + (99306 + 833q + q^2)v^{23} + (20684 + 60q)v^{24} + (3298 + 2q)v^{25} + 379v^{26} + 28v^{27} + v^{28},$$

$$C = 99q^6v^8 + (2871q^5 + 29q^6)v^9 + (36285q^4 + 2250q^5)v^{10} + (256785q^3 + 47886q^4 + 765q^5)v^{11} + (1078677q^2 + 489164q^3 + 30525q^4 + 135q^5)v^{12} + (2567538q + 2747088q^2 + 463617q^3 + 11898q^4 + 9q^5)v^{13} + (2723220 + 8371674q + 3520566q^2 + 282843q^3 + 2919q^4)v^{14} + (11070162 + 13828185q + 2965938q^2 + 120355q^3 + 420q^4)v^{15} + (22921893 + 15205050q + 1805958q^2 + 36504q^3 + 27q^4)v^{16} + (31898508 + 12327042q + 826827q^2 + 7773q^3)v^{17} + (33199952 + 7729828q + 287940q^2 + 1098q^3)v^{18} + (27253662 + 3833517q + 75627q^2 + 90q^3)v^{19} + (18157536 + 1513779q + 14556q^2 + 3q^3)v^{20} + (9965342 + 473460q + 1938q^2)v^{21} + (4531923 + 115287q + 159q^2)v^{22} + (1706052 + 21150q + 6q^2)v^{23} + (527795 + 2757q)v^{24} + (132300 + 228q)v^{25} + (26256 + 9q)v^{26} + 3976v^{27} + 432v^{28} + 30v^{29} + v^{30} \quad \text{(A.4)}$$

2. Potts model on $n\times n$ subnets with pure three-site coupling M

$$m = e^M - 1$$

Subnet 1×1:

$$A = 1, \quad B = 0, \quad C = m. \quad \text{(A.5)}$$

Subnet 2×2:

$$A = q^3 + 3qm, \quad B = m^2, \quad C = m^3. \quad \text{(A.6)}$$

Subnet 3×3:

$$A = q^7 + 6q^5m + 15q^3m^2 + (14q + 3q^2)m^3 + 3m^4,$$

$$B = q^2m^3 + (2 + 2q)m^4 + m^5,$$

$$C = 3m^5 + m^6. \tag{A.7}$$

Subnet 4×4:

$$A = q^{12} + 10q^{10}m + 45q^8m^2 + (114q^6 + 6q^7)m^3 + (165q^4 + 42q^5)m^4 + (117q^2 + 99q^3 + 9q^4)m^5 + (20 + 73q + 33q^2 + 3q^3)m^6 + (15 + 13q)m^7 + 3m^8,$$

$$B = q^5m^4 + (6q^3 + 3q^4)m^5 + (9q + 15q^2 + 3q^3)m^6 + (12 + 12q + 3q^2)m^7 + (6 + 2q)m^8 + m^9$$

$$C = (2 + 9q)m^7 + (15 + 3q)m^8 + 7m^9 + m^{10}. \tag{A.8}$$

Subnet 5×5:

$$A = q^{18} + 15q^{16}m + 105q^{14}m^2 + (445q^{12} + 10q^{13})m^3 + (1245q^{10} + 120q^{11})m^4 + (2358q^8 + 624q^9 + 18q^{10})m^5 + (2967q^6 + 1795q^7 + 189q^8 + 6q^9)m^6 + (2298q^4 + 2976q^5 + 792q^6 + 84q^7)m^7 + (888q^2 + 2613q^3 + 1608q^4 + 399q^5 + 27q^6)m^8 + (86 + 864q + 1416q^2 + 808q^3 + 182q^4 + 9q^5)m^9 + (249 + 579q + 345q^2 + 81q^3 + 3q^4)m^{10} + (126 + 129q + 36q^2)m^{11} + (30 + 13q)m^{12} + 3m^{13},$$

$$B = q^9m^5 + (12q^7 + 4q^8)m^6 + (47q^5 + 42q^6 + 6q^7)m^7 + (80q^3 + 156q^4 + 57q^5 + 7q^6)m^8 + (42q + 221q^2 + 204q^3 + 59q^4 + 7q^5)m^9 + (67 + 225q + 169q^2 + 58q^3 + 5q^4)m^{10} + (105 + 121q + 37q^2 + 5q^3)m^{11} + (49 + 25q + 3q^2)m^{12} + (11 + 2q)m^{13} + m^{14},$$

$$C = (12q^2 + 29q^3)m^9 + (6 + 63q + 96q^2 + 9q^3)m^{10} + (102 + 132q + 36q^2)m^{11} + (127 + 51q + 3q^2)m^{12} + (57 + 6q)m^{13} + 12m^{14} + m^{15}. \tag{A.9}$$

Subnet 6×6:

$$A = q^{25} + 21q^{23}m + 210q^{21}m^2 + (1315q^{19} + 15q^{20})m^3 + (5715q^{17} + 270q^{18})m^4 + (18084q^{15} + 2235q^{16} + 30q^{17})m^5 + (42560q^{13} + 11166q^{14} + 525q^{15} + 10q^{16})m^6 + (74769q^{11} + 37113q^{12} + 4113q^{13} + 210q^{14})m^7 + (96819q^9 + 85161q^{10} + 18795q^{11} + 1926q^{12} + 54q^{13})m^8 + (89350q^7 + 135082q^8 + 54561q^9 + 10086q^{10} + 798q^{11} + 18q^{12})m^9 + (54795q^5 + 143112q^6 + 102321q^7 + 32634q^8 + 5172q^9 + 351q^{10} + 6q^{11})m^{10} + (19257q^3 + 92445q^4 + 118923q^5 + 65685q^6 + 18570q^7 + 2622q^8 + 174q^9)m^{11} + (2642q + 29213q^2 + 74961q^3 + 76633q^4 + 38522q^5 + 9990q^6 + 1452q^7 + 66q^8)m^{12} + (2106 + 17556q + 41547q^2 + 42069q^3 + 20271q^4 + 5523q^5 + 735q^6 + 27q^7)m^{13} + (4536 + 16626q + 18789q^2 + 10158q^3 + 2817q^4 + 381q^5 + 9q^6)m^{14} + (3459 + 6819q + 4372q^2 + 1398q^3 + 179q^4 + 3q^5)m^{15} + (1398 + 1593q + 594q^2 + 87q^3)m^{16} + (342 + 216q + 36q^2)m^{17} + (48 + 13q)m^{18} + 3m^{19},$$

$$B = q^{14}m^6 + (20q^{12} + 5q^{13})m^7 + (145q^{10} + 90q^{11} + 10q^{12})m^8 + (540q^8 + 623q^9 + 168q^{10} + 14q^{11})m^9 + (1142q^6 + 2263q^7 + 1132q^8 + 221q^9 + 17q^{10})m^{10} + (1304q^4 + 4549q^5 + 4089q^6 + 1413q^7 + 258q^8 + 16q^9)m^{11} + (659q^2 + 4573q^3 + 7808q^4 + 4873q^5 + 1569q^6 + 238q^7 + 16q^8)m^{12} + (68 + 1652q + 6525q^2 + 8325q^3 + 4896q^4 + 1432q^5 + 214q^6 + 14q^7)m^{13} + (1183 + 4981q + 6786q^2 + 3999q^3 + 1184q^4 + 182q^5 + 11q^6)m^{14} + (1950 + 4062q + 2733q^2 + 885q^3 + 141q^4 + 9q^5)m^{15} + (1372 + 1566q + 571q^2 + 102q^3 + 7q^4)m^{16} + (538 + 338q + 64q^2 + 5q^3)m^{17} + (127 + 40q + 3q^2)m^{18} + (17 + 2q)m^{19} + m^{20},$$

$$C = (54q^5 + 99q^6)m^{11} + (146q^3 + 585q^4 + 483q^5 + 29q^6)m^{12} + (90q + 888q^2 + 1971q^3 + 1170q^4 + 159q^5)m^{13} + (228 + 1992q + 3303q^2 + 2073q^3 + 381q^4 + 9q^5)m^{14} + (1677 + 3726q + 2598q^2 + 660q^3 + 33q^4)m^{15} + (2421 + 2511q + 810q^2 + 81q^3)m^{16} + (1626 + 813q + 114q^2 + 3q^3)m^{17} + (620 + 133q + 6q^2)m^{18} + (141 + 9q)m^{19} + 18m^{20} + m^{21}. \tag{A.10}$$

Subnet 7×7:

$$A = q^{33} + 28q^{31}m + 378q^{29}m^2 + (3255q^{27} + 21q^{28})m^3 + (19950q^{25} + 525q^{26})m^4 + (92025q^{23} + 6210q^{24} + 45q^{25})m^5 + (329615q^{21} + 45955q^{22} + 1155q^{23} + 15q^{24})m^6 + (932792q^{19} + 237060q^{20} + 13755q^{21} + 430q^{22})m^7 + (2102508q^{17} + 899163q^{18} + 100401q^{19} + 5835q^{20} + 90q^{21})m^8 + (3777012q^{15} + 2577591q^{16} + 499731q^{17} + 48899q^{18} + 2062q^{19} + 30q^{20})m^9 + (5372928q^{13} + 5650464q^{14} + 1784592q^{15} + 278639q^{16} + 22401q^{17} + 846q^{18} + 10q^{19})m^{10} + (5963664q^{11}$$

$$+ 9467118q^{12} + 4680099q^{13} + 1127826q^{14} + 150330q^{15} + 10692q^{16} + 396q^{17})m^{11} + (5030270q^{9} + 11966359q^{10} + 9054966q^{11} + 3301756q^{12} + 683417q^{13} + 80559q^{14} + 5754q^{15} + 132q^{16})m^{12} + (3081149q^{7} + 11079301q^{8} + 12758268q^{9} + 6987391q^{10} + 2179863q^{11} + 399888q^{12} + 46751q^{13} + 2766q^{14} + 54q^{15})m^{13} + (1263348q^{5} + 7101903q^{6} + 12629796q^{7} + 10471011q^{8} + 4893192q^{9} + 1358682q^{10} + 242670q^{11} + 26103q^{12} + 1422q^{13} + 18q^{14})m^{14} + (294802q^{3} + 2824768q^{4} + 8154549q^{5} + 10567810q^{6} + 7525012q^{7} + 3161463q^{8} + 844184q^{9} + 144491q^{10} + 15006q^{11} + 690q^{12} + 6q^{13})m^{15} + (25948q + 547184q^{2} + 2935194q^{3} + 6464096q^{4} + 7397804q^{5} + 4847082q^{6} + 1962007q^{7} + 511413q^{8} + 86643q^{9} + 8408q^{10} + 348q^{11})m^{16} + (23688 + 392541q + 1878534q^{2} + 3986040q^{3} + 4432011q^{4} + 2878479q^{5} + 1160562q^{6} + 304893q^{7} + 50895q^{8} + 4761q^{9} + 153q^{10})m^{17} + (112270 + 781871q + 1899615q^{2} + 2296835q^{3} + 1561921q^{4} + 654696q^{5} + 175858q^{6} + 29445q^{7} + 2616q^{8} + 66q^{9})m^{18} + (162018 + 662861q + 987349q^{2} + 764529q^{3} + 345520q^{4} + 97287q^{5} + 16524q^{6} + 1404q^{7} + 27q^{8})m^{19} + (123912 + 327444q + 320334q^{2} + 166830q^{3} + 50811q^{4} + 8838q^{5} + 747q^{6} + 9q^{7})m^{20} + (60508 + 106552q + 69966q^{2} + 24288q^{3} + 4547q^{4} + 372q^{5} + 3q^{6})m^{21} + (20268 + 23740q + 10182q^{2} + 2142q^{3} + 188q^{4})m^{22} + (4710 + 3525q + 894q^{2} + 87q^{3})m^{23} + (732 + 316q + 36q^{2})m^{24} + (69 + 13q)m^{25} + 3m^{26},$$

$$B = q^{20}m^{7} + (30q^{18} + 6q^{19})m^{8} + (345q^{16} + 165q^{17} + 15q^{18})m^{9} + (2175q^{14} + 1820q^{15} + 390q^{16} + 25q^{17})m^{10} + (8587q^{12} + 11240q^{13} + 4199q^{14} + 624q^{15} + 35q^{16})m^{11} + (22421q^{10} + 43891q^{11} + 25772q^{12} + 6546q^{13} + 844q^{14} + 40q^{15})m^{12} + (38966q^{8} + 113011q^{9} + 100896q^{10} + 39578q^{11} + 8607q^{12} + 951q^{13} + 43q^{14})m^{13} + (43431q^{6} + 190110q^{7} + 258498q^{8} + 153642q^{9} + 50665q^{10} + 9597q^{11} + 981q^{12} + 44q^{13})m^{14} + (28116q^{4} + 196731q^{5} + 420318q^{6} + 385688q^{7} + 190950q^{8} + 55686q^{9} + 9626q^{10} + 970q^{11} + 40q^{12})m^{15} + (8320q^{2} + 108004q^{3} + 395182q^{4} + 590541q^{5} + 455390q^{6} + 203444q^{7} + 54523q^{8} + 9175q^{9} + 874q^{10} + 37q^{11})m^{16} + (488 + 20976q + 170827q^{2} + 477931q^{3} + 626376q^{4} + 452018q^{5} + 190124q^{6} + 50024q^{7} + 8064q^{8} + 775q^{9} + 32q^{10})m^{17} + (15646 + 137655q + 396335q^{2} + 531376q^{3} + 381398q^{4} + 162295q^{5} + 42103q^{6} + 6904q^{7} + 640q^{8} + 28q^{9})m^{18} + (51536 + 224439q + 352647q^{2} + 280816q^{3} + 123719q^{4} + 33731q^{5} + 5505q^{6} + 532q^{7} + 22q^{8})m^{19} + (66881 + 176633q + 170578q^{2} + 86821q^{3} + 24401q^{4} + 4339q^{5} + 407q^{6} + 18q^{7})m^{20} + (49197 + 83330q + 51390q^{2} + 17058q^{3} + 3016q^{4} + 326q^{5} + 13q^{6})m^{21} + (23535 + 25741q + 10127q^{2} + 2132q^{3} + 217q^{4} + 11q^{5})m^{22} + (7727 + 5333q + 1281q^{2} + 155q^{3} + 7q^{4})m^{23} + (1751 + 719q + 94q^{2} + 5q^{3})m^{24} + (264 + 57q + 3q^{2})m^{25} + (24 + 2q)m^{26} + m^{27},$$

$$C = (222q^{9} + 351q^{10})m^{13} + (1386q^{7} + 3816q^{8} + 2250q^{9} + 99q^{10})m^{14} + (3198q^{5} + 14696q^{6} + 18894q^{7} + 7530q^{8} + 686q^{9})m^{15} + (3072q^{3} + 24933q^{4} + 59031q^{5} + 51366q^{6} + 18519q^{7} + 2208q^{8} + 29q^{9})m^{16} + (888q + 16710q^{2} + 78501q^{3} + 132330q^{4} + 99747q^{5} + 35370q^{6} + 5022q^{7} + 150q^{8})m^{17} + (1954 + 32712q + 133203q^{2} + 202318q^{3} + 150051q^{4} + 55086q^{5} + 8997q^{6} + 456q^{7})m^{18} + (25370 + 130809q + 228960q^{2} + 178833q^{3} + 72045q^{4} + 13566q^{5} + 948q^{6} + 9q^{7})m^{19} + (67692 + 179352q + 174174q^{2} + 78354q^{3} + 17760q^{4} + 1581q^{5} + 33q^{6})m^{20} + (81987 + 127689q + 73398q^{2} + 19325q^{3} + 2343q^{4} + 72q^{5})m^{21} + (58543 + 54880q + 18612q^{2} + 2746q^{3} + 150q^{4})m^{22} + (27453 + 15033q + 2859q^{2} + 207q^{3} + 3q^{4})m^{23} + (8825 + 2607q + 246q^{2} + 6q^{3})m^{24} + (1949 + 264q + 9q^{2})m^{25} + (285 + 12q)m^{26} + 25m^{27} + m^{28}. \quad \text{(A.11)}$$

[1] R. B. Potts, Proc. Cambridge Phys. Soc. **48**, 106 (1952).
[2] F. Y. Wu, Rev. Mod. Phys. **54**, 235 (1982).
[3] M. P. M. den Nijs, J. Phys. A **12**, 1857 (1979).
[4] J. L. Black and V. J. Emery, Phys. Rev. B **23**, 429 (1981).
[5] B. Nienhuis, E. K. Riedel, and M. Schick, J. Phys. A **13**, L31 (1980).
[6] B. Nienhuis, A. N. Berker, E. K. Riedel, and M. Schick, Phys. Rev. Lett. **43**, 737 (1979).
[7] M. P. M. den Nijs, Phys. Rev. B **27**, 1674 (1983).
[8] R. B. Griffiths, Phys. Rev. Lett. **24**, 1479 (1970).
[9] F. Y. Wu, Phys. Rev. E **81**, 061110 (2010).
[10] A. Haji-Akbari and R. M. Ziff, Phys. Rev. E **79**, 021118

(2009).
[11] R. M. Ziff and H. Gu, Phys. Rev. E **79**, 020102(R) (2009).
[12] F. Y. Wu, Phys. Rev. Lett. **96**, 090602 (2006).
[13] C. M. Fortuin and P. W. Kasteleyn, Physica **57**, 536 (1972).
[14] P. W. Kasteleyn and C. M. Fortuin, J. Phys. Soc. Jpn. **26**, (Suppl.), 11 (1969).
[15] F. Y. Wu and H. Y. Huang, Phys. Rev. Lett. **79**, 4954 (1997).
[16] H. N. V. Temperley and E. H. Lieb, Proc. R. Soc. London, Ser. A **322**, 251 (1971).
[17] H. W. J. Blöte and M. P. Nightingale, Physica A **112**, 405 (1982).
[18] H. W. J. Blöte and B. Nienhuis, J. Phys. A **22**, 1415 (1989).
[19] X.-F. Qian, Y. Deng, and H. W. J. Blöte, Phys. Rev. E **72**, 056132 (2005).
[20] W.-A. Guo, Y. Deng, and H. W. J. Blöte, Phys. Rev. E **79**, 061112 (2009).
[21] W.-A. Guo, X.-F. Qian, H. W. J. Blöte, and F. Y. Wu, Phys. Rev. E **73**, 026104 (2006).
[22] B. Li, W.-A. Guo, and H. W. J. Blöte, Phys. Rev. E **78**, 021128 (2008).
[23] W.-A. Guo, B. Nienhuis, and H. W. J. Blöte, Phys. Rev. Lett. **96**, 045704 (2006).
[24] W.-A. Guo, H. W. J. Blöte, and F. Y. Wu, Phys. Rev. Lett. **85**, 3874 (2000).
[25] X.-M. Feng, Y. Deng, and H. W. J. Blöte, Phys. Rev. E **78**, 031136 (2008).
[26] For reviews, see e.g., M. P. Nightingale, in *Finite-Size Scaling and Numerical Simulation of Statistical Systems*, edited by V. Privman (World Scientific, Singapore, 1990); M. N. Barber in *Phase Transitions and Critical Phenomena*, edited by C. Domb and J. L. Lebowitz (Academic, New York, 1983), Vol. 8.
[27] J. L. Cardy, J. Phys. A **17**, L385 (1984).
[28] H. W. J. Blöte, J. L. Cardy, and M. P. Nightingale, Phys. Rev. Lett. **56**, 742 (1986).
[29] I. Affleck, Phys. Rev. Lett. **56**, 746 (1986).
[30] B. Nienhuis, in *Phase Transitions and Critical Phenomena*, edited by C. Domb and J. Lebowitz (Academic, London, 1987), Vol. 11.
[31] J.-A. Chen, C.-K. Hu, and F. Y. Wu, J. Phys. A **31**, 7855 (1998).
[32] P. M. Ziff and P. N. Suding, J. Phys. A **30**, 5351 (1997).
[33] C. R. Scullard and R. M. Ziff, Phys. Rev. E **73**, 045102(R) (2006).
[34] R. Parviainen, J. Phys. A: Math. Theor. **40**, 9253 (2007).
[35] F. Y. Wu, J. Phys. C **12**, L645 (1979).
[36] C. R. Scullard and R. M. Ziff, J. Stat. Mech.: Theory Exp. (2010) P03021
[37] P. N. Suding and R. M. Ziff, Phys. Rev. E **60**, 275 (1999).
[38] M. F. Sykes and J. W. Essam, J. Math. Phys. **5**, 1117 (1964).
[39] R. M. Ziff, Phys. Rev. E **73**, 016134 (2006).